
Article:
Priest, J., Ghadbeigi, H., Avar-Soberanis, S. et al. (1 more author) (2021) 3D finite element modelling of drilling: the effect of modelling method. CIRP Journal of Manufacturing Science and Technology, 35. pp. 158-168. ISSN 1755-5817

https://doi.org/10.1016/j.cirpj.2021.06.001

3D Finite Element Modelling of Drilling: The Effect of Modelling Method

Joshua Priest [a,b], Hassan Ghadbeigi [b], Sabino Avar-Soberanis [c], Stefanos Gerardis [d,e]

[a] Industrial Doctoral Centre in Machining Science, Advanced Manufacturing Research Centre with Boeing, University of Sheffield, Rotherham, S60 5TZ, UK
[b] The University of Sheffield, Department of Mechanical Engineering, Sir Fredrick Mappin Building, Mappin Street, S1 3JD, Sheffield, UK
[c] Advanced Manufacturing Research Centre with Boeing, Advanced Manufacturing Park, Catcliffe, Rotherham, S60 5TZ, UK
[d] Sandvik Coromant, Morse Way, Rotherham, S60 5BJ, UK
[e] University of Western Macedonia, Department of Mechanical Engineering, Bakola & Sialvera Street, 50132 Kozani, Greece

Abstract

A comprehensive benchmarking study has been carried out to determine the influence of the mesh formulation and chip separation methods on the reliability and accuracy of finite element modelling of large diameter drilling operations. The Coupled Eulerian-Lagrangian and the updated-Lagrangian (with element deletion) formulations available in ABAQUS/Explicit, together with the updated-Lagrangian (with re-meshing) formulation in DEFORM 3D are compared by simulating through-coolant drilling of AISI 1045. The Johnson-Cook damage model was implemented by a sub-routine in DEFORM 3D to ensure a consistent damage model is implemented across the formulations. Experimentally measured drilling thrust force, torque, and chip thickness values were used to compare the models performance and assess the accuracy of the predictions. The updated-Lagrangian with dynamic re-meshing was found to be the best performing methodology concerning the accuracy of predictions, whilst the Coupled Eulerian-Lagrangian methodology significantly under-predicted the drilling thrust force and torque. Due to numerical instabilities and computational cost, the updated-Lagrangian with element deletion method is not recommended to model large diameter drilling.

Keywords: Finite Element, Mesh Formulation, Chip Separation, Drilling, CEL,

Nomenclature

Notation	Description	Units
ε_p	Equivalent Plastic Strain	--
$\dot{\varepsilon}_p$	Equivalent Plastic Strain Rate	s^{-1}
ε_f	Equivalent Plastic Strain at Fracture	--
T	Temperature	°C
T_m	Melting Temperature	°C
T_0	Johnson-Cook Reference Temperature	°C
σ	Von-Mises Equivalent Flow Stress	MPa
σ_m	Hydrostatic Stress	MPa
D	Damage	--
L	Element Characteristic Length	mm
u_f	Displacement to Failure	mm
A, B, C, m, n	Johnson-Cook Constitutive Model Coefficients	--
$d_1 - d_5$	Johnson-Cook Damage Model Coefficients	--
τ_f	Frictional Shear Stress	MPa
σ_n	Normal Contact Pressure	MPa
μ	Coefficient of Friction	
m	Coefficient of Frictional Limiting Shear Stress	
σ_y	Uniaxial Yield Stress	MPa

1 Introduction

Drilling accounts for more than 50 % of all total machining operations in the aerospace and automotive industries [1]. Controlling the quality of the produced holes with respect to the surface integrity and geometrical accuracy, whilst maximising production rates and tool life is of critical importance. Therefore, to design new tools to meet these growing demands, a more detailed understanding of the mechanics of cutting with respect to tool geometries, cutting conditions, and workpiece materials is needed. Along with experimental investigations, numerical modelling methods such as finite element modelling have been widely implemented to meet this demand.

Drilling is a complex process, whereby 3D modelling is required to represent the tool geometry and severity of material deformation. The updated-Lagrangian mesh formulation is commonly implemented for modelling such operations as it is used in DEFORM [2], AdvantEdge [3], and Abaqus/Explicit [4], which are the most popular finite element (FE) software packages for modelling machining operations [5]–[7]. This formulation must be combined with a method to separate the chip from the workpiece material and prevent excessive mesh distortion. Although, there are several challenges involved in implementing an adequate separation criteria as the fundamental mechanism of chip formation is still unknown and largely debated in literature [8],[9]. The chip separation method based upon pure-deformation that requires dynamic re-

meshing to prevent excessive mesh deformation [9], and the physical separation criteria [10] have both been widely implemented in 3D drilling simulations in the literature [5]–[7]. The latter requires a reliable damage and fracture model to degrade and delete the element from the simulation [10].

The Coupled Eulerian-Lagrangian (CEL) mesh formulation has been implemented in orthogonal cutting simulations [11], [12], and more recently is being implemented to study chip segmentation [13] and to consider the fluid-structure interaction of the chip with coolant [14]. Although, the literature concerning the simulation of complex 3D machining operations is limited [15], [16], especially concerning drilling [17]. Unlike traditional Eulerian simulations [18], this newly developed method does not require the initial chip geometry to be defined [19]. This CEL formulation has already been compared with the updated-Lagrangian formulation with element deletion when modelling 3D drilling [17], showing a more accurate prediction of the thrust force and chip geometry with a considerable reduction in simulation time. However, no chip formation was reported in the updated-Lagrangian formulation as a course 100μm element size was used, this significantly impacts the accuracy of the model. A comparative study simulating the orthogonal cutting process [11] reported that, although the CEL formulation underestimates the cutting forces compared with the experimental data, it was still more accurate than the updated-Lagrangian formulation with dynamic re-meshing in AdvantEdge and DEFORM. The CEL formulation was found to predict higher temperatures than updated-Lagrangian formulation leading to the under-prediction of cutting forces due to thermal softening, as also reported Zhang et al. [20].

Considering the complexity of deformation in the drilling process and its associated numerical challenges when modelling large diameter (i.e. >3 mm) drilling operations, the applied mesh formulation and chip separation method plays a critical role on the performance of the model. To the best knowledge of the authors there is no comprehensive comparative study on the effect of mesh formulation and chip separation methods, which includes the updated-Lagrangian with dynamic re-meshing and CEL formulations, for modelling drilling operations.

The present study aims to investigate the reliability of the available mesh formulation and chip separation methods for modelling 3D drilling operations in metallic materials. The behaviour of the CEL and updated-Lagrangian with dynamic re-meshing formulations at the onset and evolution of material damage has also not been studied. Therefore, this study will isolate the effect of the damage model in these formulations for direct comparison. The performance of

these models is assessed with respect to the accuracy of their predictions, compared with the experimentally measured thrust force, torque, and chip geometry, as well as their computational cost.

2 Experimental Drilling Study

Two 7.49mm diameter Sandvik CoroDrill 460XM cemented carbide drill with through-coolant channels were used to drill 40 through-holes each in an AISI 1045 medium carbon steel plate at two cutting parameter sets with a 6 % concentration Hocut 795-H emulsion coolant. The tools were visually inspected and the tool wear was found to be negligible after 40 holes as this is only approximately 3 % of its recommended tool life. Images of the flank and rake faces of the tools used after 40 holes can be seen in Figure 1. The first cutting condition was the manufacturers recommended parameters with a feed rate of 816 mm/min together with an 85.5 m/min cutting speed. An additional trial was conducted at a higher cutting speed of 128.5 m/min while the feed/rev was reduced to maintain the same feed rate. The average thrust force and torque, measured using a Kistler 9170A dynamometer, from drilling 40 holes can be seen in Table 1 and representative thrust force and torque evolutions are shown in Figure 2a. The solid lines represents evolution of the thrust force and the torque evolution is demonstrated by the dashed lines.

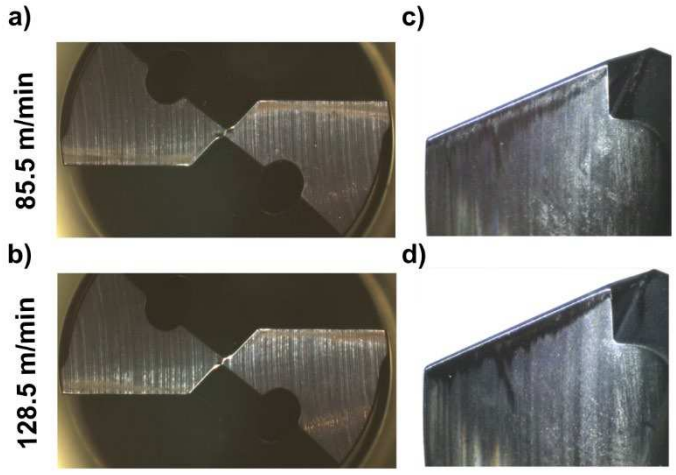

Figure 1: Tool wear scars on the flank faces (a,b) and rake faces (c,d) at both 85.5 m/min (a,c) and 128 m/min (b,d) cutting speeds.

Table 1
Average experimental cutting force and torque with an 816 mm/min feed rate

Cutting Speed (m/min)	Feed/Rev (mm/rev)	Thrust Force (N)			Torque (Nm)		
		Minimum	Maximum	Mean	Minimum	Maximum	Mean
85.5	0.224	1364.2	1499.1	1437.6	4.138	4.417	4.250
128.5	0.145	1044.2	1170.5	1105.9	2.908	3.145	2.997

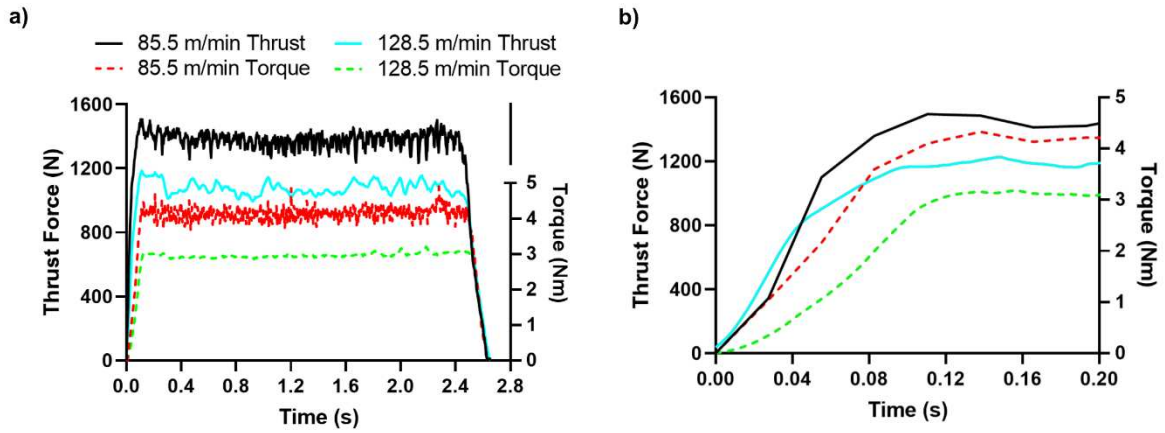

Figure 2: (a) Representative measured smoothed drilling thrust force and torque data with time in seconds at both cutting conditions reported with (b) the non-smoothed raw data at the initial tool entry part of the graph highlighted.

As the drill tip enters the workpiece the thrust force and torque rapidly increase until the point of the drill has fully penetrated the workpiece and steady-state engagement is reached where the uncut chip thickness is at its maximum. This entry is shown in Figure 2b, steady-state engagement is reached by approximately 0.12 s. As the drill tip begins to penetrate through the bottom of the workpiece these gradually decline until the drill exits the workpiece.

To quantify the chip thickness and its variation, an Alicona infinite focus microscope was used to construct a 3D image of two representative chip sections. These measurements were only carried out for the first trial at the manufacturers recommended parameter set with a cutting speed of 85.5 m/min. The minimum (T_{min}) and maximum (T_{max}) thickness of the chip that formed at the outer edge of the drill were measured. A representative chip section is shown in Figure 3a together with, the 3D reconstructed image showing the corresponding points of interest (Figure 3b), and the measured values (Figure 3c). The error bars in Figure 3c represent the variation in measurement at the T_{min} and T_{max} locations between the representative chips.

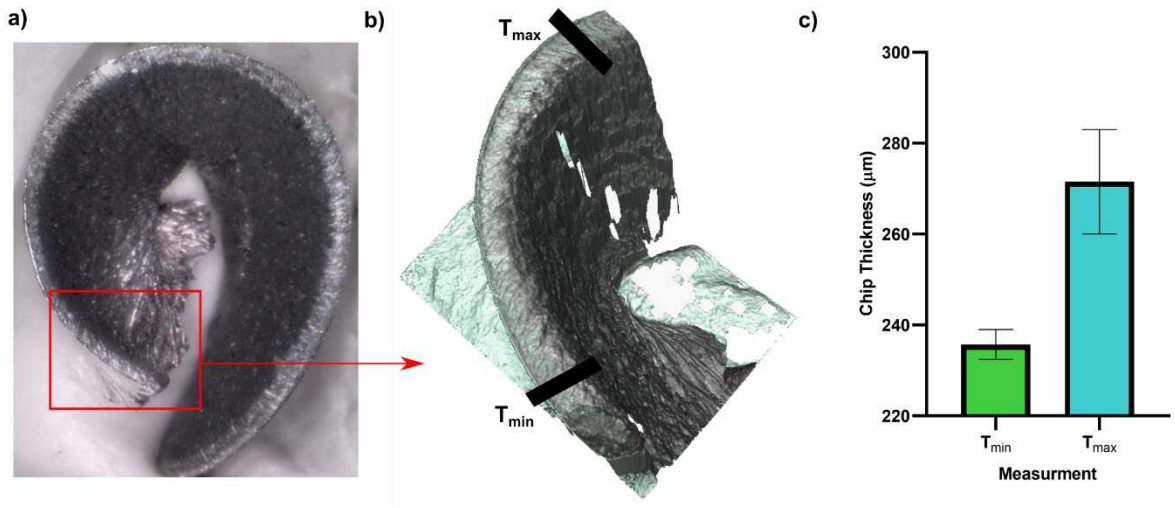

Figure 3: (a) Optical image of produced chip at 85.5 m/min cutting parameter set, (b) 3D scan image of the chip using an infinite focus microscope with the measurement locations indicated, and (c) measured chip thicknesses at position T_{min} and T_{max} at manufacturers recommended cutting speed (85.5 m/min)

3 Modelling Methodology

Table 2 details the modelling methodologies compared in this study. Due to numerical stability issues at a low mesh density, and the significant computational demands at higher mesh densities, drilling with large diameter drills (such as the tool used in this study) could not be economically modelled using the updated-Lagrangian with element deletion methodology and a coupled thermo-mechanical solver. Therefore a solely mechanical solver was used instead. Although, as this does not represent the physics of the problem, it was only used to demonstrate the behaviour of this formulation and is not directly compared to the other modelling methodologies in this study. The suitability of this method modelling 3D drilling operations is discussed in more detail in section 3.3.1.

Table 2
Modelling Methodologies Comparison Table

Software Package	Formulation	Chip Separation Method	Material Damage	Model Acronym
ABAQUS (Explicit)	updated-Lagrangian	Element Deletion	✓	u-LAG
	CEL	Not Required	✗	CEL
	CEL	Not Required	✓	CEL-DMG
DEFORM 3D (Implicit)	updated-Lagrangian	Pure Deformation	✗	u-LAG_RM
	updated-Lagrangian	Pure Deformation	✓	u-LAG_RM_DMG

The ABAQUS/Explicit and Implicit DEFORM 3D software packages were used to implement the CEL and the updated-Lagrangian with dynamic re-meshing methodologies respectively. Although it is not required to couple these methodologies with a damage and fracture model,

this was additionally implemented to in both methodologies to determine the effect of material softening due to damage.

3.1 Model Geometry

A consistent model geometry, as shown in Figure 4, was used across all simulations. The edge radius of the tools used in the experimental study were measured at multiple points on along the cutting and chisel edges and was replicated in the tool 3D CAD models. The tool is modelled as a rigid body; the physical properties of this tool and the workpiece are shown in Table 3.

Table 3
Physical properties of the workpiece and cutting tool taken from the Simufact Material Database [21]

Property	AISI 1045 Workpiece	Tungsten Carbide Tool
Young's Modulus	*Temperature Dependent*	--
Poisons Ratio	0.29	--
Density	7800 kg/m^3	14850 kg/m^3
Thermal Expansion	*Temperature Dependent*	--
Specific Heat Capacity (c_p)	*Temperature Dependent*	200 J/kg.K
Thermal Conductivity	*Temperature Dependent*	100 W/m.K

The geometrical features of the drill were used to define the workpiece geometry so that the model reaches the steady-state engagement region of the drilling process quickly after the initiation of the cut. The models simulate a total of 0.012 seconds of drilling to ensure a steady-state engagement region is reached, this is theoretically reached when the maximum uncut chip thickness is reached at 0.00825 s for the recommended cutting parameter set and at 0.0053 s for the higher cutting speed parameter set. These theoretical times to reach steady-state differ from the experimentally observed values, as shown in Figure 2b, due to the applied geometry of the workpiece in the simulation where the initial stage of drill engagement is omitted by using a cone shaped geometry to reduce the simulation time. The outer faces of the workpiece were fixed to replicate the material clamping in the experiment, preventing displacement in all degrees of freedom.

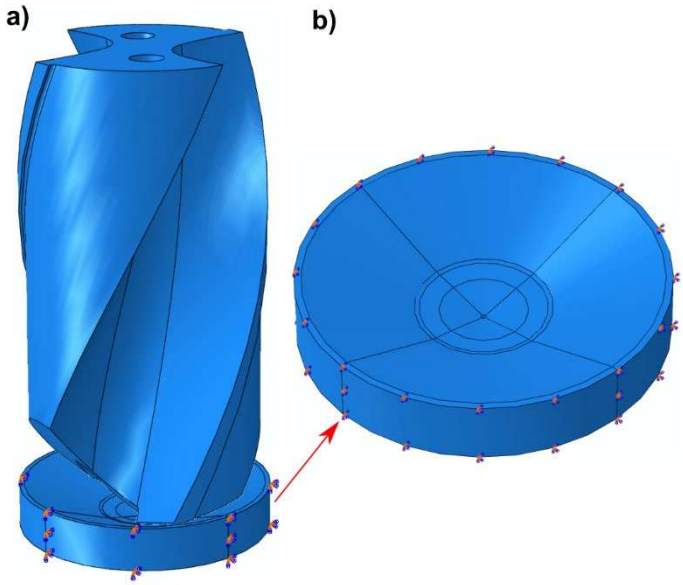

Figure 4: (a) The tool and workpiece geometry, showing the initial tool-workpiece interaction, and (b) the workpiece cone shape geometry.

3.2 Material and Friction Models

The phenomenological Johnson-Cook material constitutive model [22] (equation 1) was used to describe the workpiece material behaviour. The literature on FE modelling of 3D drilling operations almost exclusively uses this model, primarily because this is shown to predict material behaviour with reasonable accuracy within the range of experimental data used to calibrate the model [23]. To simulate the damage softening and fracture of the material, the Johnson-Cook damage initiation criteria [24] in equation 2 was implemented with the linear damage evolution model as shown in equation 3. Although more advanced models are also available, and further research into accurate damage and fracture prediction is required, this is out of the scope of the present paper.

Table 4 shows the parameters used for the implemented material constitutive and damage models, and as for the damage evolution law, a constant displacement to failure (u_f) of 0.1 mm was implemented [25]. It is also assumed that 90 % of the plastic work is converted into heat during deformation [11], [26].

$$\sigma = \left[A + B\varepsilon_p^n\right]\left[1 + C\ln\left(\frac{\dot{\varepsilon}_p}{\dot{\varepsilon}_0}\right)\right]\left[1 - \left(\frac{T - T_0}{T_m - T_0}\right)^m\right] \quad (1)$$

$$\varepsilon_f = \left[d_1 + d_2\exp\left(d_3\frac{\sigma_m}{\sigma}\right)\right]\left[1 + d_4\ln\left(\frac{\dot{\varepsilon}_p}{\dot{\varepsilon}_0}\right)\right]\left[1 + d_5\frac{T - T_0}{T_m - T_0}\right] \quad (2)$$

$$D = L\frac{\varepsilon_p}{u_f} \tag{3}$$

Table 4
Johnson Cook Constitutive [27] and Damage Model [28] Parameters

Constitutive Model	$\boldsymbol{A}$ $(\boldsymbol{MPa})$	$\boldsymbol{B}$ $(\boldsymbol{MPa})$	$\boldsymbol{C}$	$\boldsymbol{n}$	$\boldsymbol{m}$	$\dot{\boldsymbol{\varepsilon}}_{\boldsymbol{0}}$ $(\boldsymbol{s^{-1}})$	$\boldsymbol{T_0}$ (°C)	$\boldsymbol{T_m}$ (°C)
	553.1	600.8	0.013	0.234	1	1	20	1493
Damage Model	$\boldsymbol{d_1}$	$\boldsymbol{d_2}$	$\boldsymbol{d_3}$	$\boldsymbol{d_4}$	$\boldsymbol{d_5}$	$\dot{\boldsymbol{\varepsilon}}_{\boldsymbol{0}}$ $(\boldsymbol{s^{-1}})$	$\boldsymbol{T_0}$ (°C)	$\boldsymbol{T_m}$ (°C)
	0.06	3.31	-1.96	0.0018	0.58	1	20	1493

A new subroutine to implement this damage and fracture model into the DEFORM 3D software package was developed and validated. This ensures a consistent material damage model and fracture model is implemented across the DEFORM 3D and ABAQUS/Explicit software packages, limiting the studies independent variables to the mesh formulation and chip separation method.

The modified Zorev sticking-sliding friction model by Childs [29] was implemented in the simulations. This type of model has been shown to better represent the physics of the frictional shear stresses on the rake face of the tool in the secondary shear zone [30], and it considers the effects of the material thermal softening on the limiting shear stress at the cutting conditions used. Equation 4 shows the applied friction model where σ_n is the normal contact pressure on the tool, μ is the coefficient of friction, m is the Childs's constant, and σ_y is the uniaxial yield strength of the workpiece material. There are a wide range of coefficient of friction values reported in the literature for the contact between AISI 1045 and tungsten carbide [31],[7], [32], [33], however, a coefficient of friction of 0.3 with a Child's coefficient of 0.7 was used as this yielded the most accurate results in a preliminary study. It was assumed that the frictional work is fully converted into heat and is equally dissipated into the drill and the workpiece. Additional heat exchange due to the conduction of heat between the tool and the workpiece occurs with a defined thermal contact conductance of 45 kW/m^2 K, as recommended by DEFORM [34]. This is also within the range of 10 – 10,000 kW/m^2 K, which is commonly used for the tool-chip contact [35].

$$\tau_f = \begin{cases} \mu\sigma_n, & \mu\sigma_n < \mathrm{m}\,\dfrac{\sigma_y}{\sqrt{3}} \\ \mathrm{m}\,\dfrac{\sigma_y}{\sqrt{3}}, & \mu\sigma_n \geq \mathrm{m}\,\dfrac{\sigma_y}{\sqrt{3}} \end{cases} \tag{4}$$

3.3 Mesh Formulations

Some of the mesh properties and thermal considerations vary between the different modelling methodologies studied, these are explained in the following sections.

3.3.1 Updated-Lagrangian with Element Deletion Method

The workpiece was meshed using structured hexahedral reduced integration elements (C3D8R), with a similar mesh structure to that implemented by Nan et al. [7] and Hu et al. [6]. Two models with different mesh densities were developed to assess the performance of this methodology; the first had a 60 µm element size comparable to that implemented in the other methodologies resulting in 112,000 elements and a refined mesh with 10µm elements in the drill feed axis and widths ranging from 20 – 50 µm in the radial direction was used in the second model, resulting in 695,520 elements as shown in Figure 5. Additionally, as there is also no consideration for coolant in this simulation due to lack of thermal modelling, one would have to assume that the coolant carries all the heat away for this model to be valid, that is neither a valid assumption, nor does it represent the physics of the problem.

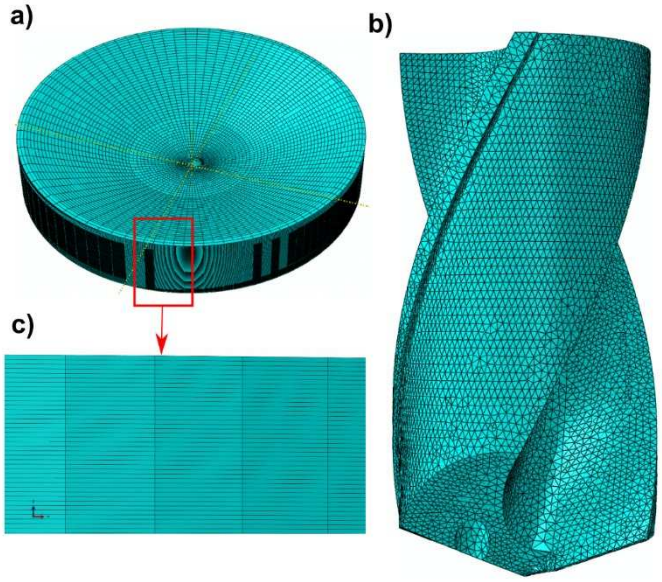

Figure 5: Mesh morphology of the updated-Lagrangian modelling showing the variation of element sizes in the (a, c) workpiece and (b) the drill. The element size was constant in the drill feed direction as shown in (c).

This u-LAG model was very computationally intensive during a thermo-mechanically coupled simulation, after 336 hours of simulation time on a 20 core Intel Xeon Gold 6138 processor the drill in the model was still yet to reach full engagement. This was even the case after a large mass scaling factor of 2000 was used to artificially increase the time increments, increasing the mass scaling factor beyond this caused the model to become unstable and the kinetic energy to exceed the recommended 5 – 10 % of the total energy [36]. A reduction of mesh density, in

order to reduce the simulation time, caused the premature failure of the model due to numerical instability caused by excessive mesh distortion around the chisel edge of the drill. Additionally, application of any distortion control or artificially amending the damage evolution model to encourage earlier deletion of the element was neither successful nor does it accurately represent the mechanics of the deformation.

Although it is reported that the updated-Lagrangian with element deletion methodology can be applied for 3D modelling of the drilling operation, these models were either used to simulate small drill diameters of about 3 mm [7] or with very coarse mesh morphologies for larger diameter drills up to 8 mm without a thermally-coupled solver [6], [32], [37]. The coarse mesh used in the latter does not cause excessive mesh distortion errors as the thermal softening effect is neglected. The mesh requirements necessary to implement the updated-Lagrangian with element deletion methodology with a thermally-coupled solver to model large diameter drilling, as in this study, is beyond what can be expected from a typical high-performance computing facility. Therefore, this methodology it is only computationally economical for thermo-mechanical modelling of small diameter (up to 3 mm) drilling operations.

3.3.2 CEL Method

In the CEL methodology the Eulerian domain, where the workpiece material flows, was defined as a 7.79 mm x 7.79 mm x 3.218 mm cube surrounding the drill, as shown by the red region in Figure 6a, to ensure there is enough space to model the chip formation. The workpiece geometry was defined (Figure 6b) and embedded within the Eulerian domain, as shown by the blue region in Figure 6a. This Eulerian domain is then meshed with 60 µm cubed thermally-coupled reduced integration EC3D8RT structured elements, as shown in Figure 6c, resulting in a total of 877,000 elements.

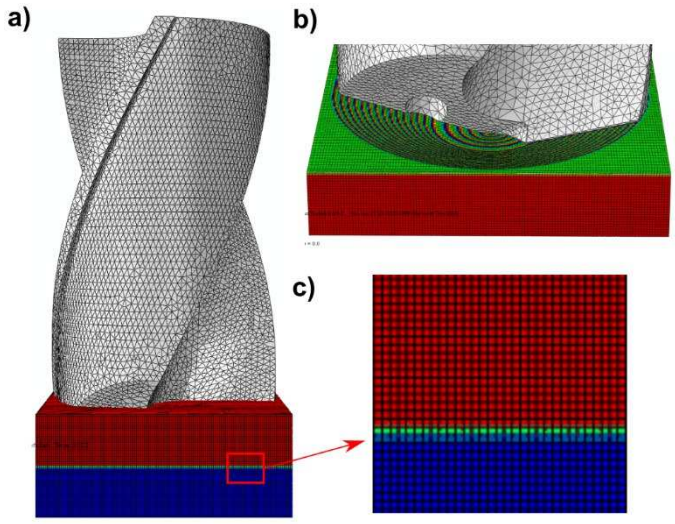

Figure 6: (a) The CEL model geometry indicating Eulerian domain in red and the initial workpiece in blue, (b) the same cone shape geometry as used previously is implemented and (c) 60µm cubed elements are used to mesh the Eulerian domain.

To account for the convective heat transfer of the coolant, in this model, a 20 °C isothermal boundary condition is applied to the outer faces to act as a thermal sink. It is not possible to apply a convection boundary condition to the initial workpiece geometry, as it is not possible to apply boundary conditions to internal elements and nodes within the Eulerian domain.

3.3.3 Updated-Lagrangian with Re-Meshing Method

The same workpiece geometry as that used in the u-LAG model was used (Figure 4). The initial mesh morphology of the workpiece contained 210,000 thermally-coupled unstructured elements with dynamic re-meshing enabled. Precise control of the element sizes in this methodology is not possible due to the limited control over the software. However, the element sizes varied between about 40µm and 80 µm in the primary and secondary shear zones to make it approximately comparable to the 60 µm structured elements used in the CEL models. An isothermal boundary condition at 20 °C is applied to the outer faces of the workpiece to simulate the thermal effects of coolant and ensure consistency in the thermal consideration with the CEL models.

As the elasto-plastic solver used in DEFORM does not account for strain-rate hardening [34], a pure plastic modelling approach was adopted to account for strain and strain-rate hardening at a cost of ignoring the elastic deformation of the workpiece. Additionally, in contrast to the ABAQUS/Explicit solver, an implicit time integration method is used in DEFORM that allows the time step to be much larger whilst remaining numerically stable.

In this method, instead of using element deletion, the material failure is simulated by reducing the flow stress of damaged elements to 1 % of its capacity based on the Johnson-Cook flow rule. Additionally, as there is no way to gradually degrade the element load capacity in DEFORM 3D, the element is softened instantaneously upon satisfaction of the failure criteria. This implementation is as consistent as is possible between the software packages due to software limitations in DEFORM 3D.

4 Results and Discussion

The performance of the applied methods to model the drilling process are assessed based on the accuracy of the predicted thrust force, torque, and chip geometry, and computational time. Additionally, the temperature prediction of each methodology is compared, although this is not compared to experimental data.

4.1 Thrust Force and Torque Prediction

Figure 7a to Figure 7d shows the predicted evolutions of the drilling thrust force and torque by all the applied methodologies compared with the experimentally measured data. The evolutions of the predicted thrust force and torque are shown by the black and red lines respectively, whilst the green and light blue bands represent the range of the experimentally measured values during the steady-state engagement region, respectively. The dashed lines in Figure 7a and 7b show the predicted thrust force and torque evolutions with the addition of the damage model. The average steady-state engagement errors of each model are then shown in Figure 7e, the error bars represent the variation in the error of the predicted finite element steady-state forces compared with the minimum and maximum steady-state forces experimentally measured across 40 holes; these experimental minimum and maximum values are presented in Table 1.

The u-LAG_RM and u-LAG_RM _DMG models, in Figure 7a, were the most accurate models with both the thrust and torque predictions within 15 % of the experimental steady-state engagement values. The implementation of material damage in the u-LAG_RM _DMG model did not impact the steady state predicted thrust force or torque. This is because the damage evolution in the u-LAG_RM _DMG did not consistently exceed the critical value (1) to initiate material softening. The predicted torque evolution in both the u-LAG_RM and u-LAG_RM_DMG models agrees very well with the torque evolution seen in the experiment (Figure 2b) with its magnitude gradually increasing until a steady-state torque and maximum chip thickness is reached at approximately 0.00825 s. The thrust force begins to reduce at this time step and reaches a steady-state later in the simulation at approximately 0.01 s. This decrease in the thrust force can be seen in the experimental data (Figure 2), but the models predict maximum thrust value much larger than what is observed in the experiment. This effect is potentially related to the increased rate of heat build-up causing thermal softening when the torque and chip load reaches their maximum value. This trend in the evolution of the thrust force was not observed in the CEL and CEL-DMG models, these models in this regard shows a better agreement with the experimental force evolution.

Figure 7b shows the results of the CEL and CEL-DMG models respectively, both of which significantly under predicted the thrust force and torque compared with the experimentally measured values. A similar trend has been previously reported when using the CEL formulation to model 3D drilling [17] and 2D orthogonal cutting [11], [38]. The implementation of material damage in the CEL formulation deteriorated the models thrust force and torque prediction by

a further 30 % that could be linked to the model predicting a fully damaged layer of elements (softened to 1 % of their flow stress) beneath the tool.

The differences in the impact of implementing material damage in the CEL and updated-Lagrangian with dynamic re-meshing formulations is likely linked to the differences in the applied element types and the potential for variation in the characteristic lengths (L) of the elements due to the use of re-meshing in the updated-Lagrangian with dynamic re-meshing formulation. The latter was minimised as much as possible by controlling the element sizes in the deformation zones to within ± 20 µm of the 60 µm element size (comparable to that used in the CEL formulation), although this unavoidable variation will impact the damage evolution rate, with slightly larger elements softening and reaching their fully deteriorated state at a much higher rate compared to smaller elements with the same displacement to failure value (u_f). This potentially caused the damage in the elements beneath the tool evolved at a much higher rate in the CEL-DMG model, resulting in the layer of fully damaged elements which was not observed in the u-LAG_RM_DMG model.

This demonstrates the mesh dependency of the implemented damage and fracture model, and the importance of tuning the displacement to failure value (u_f) to the element size for 3D drilling simulations. The mesh dependency effect was minimised as much as possible by controlling the element size in the u-LAG_RM_DMG model to make it comparable to the CEL-DMG model, although this could not be eliminated due to the evolving characteristic element length caused by dynamic re-meshing.

The u-LAG model with a 60 µm element size, consistent with that used in the CEL and updated-Lagrangian with re-meshing methodologies did not produce a chip (discussed in section 4.2), leading to the physically meaningless force response, therefore this is discounted and not discussed further. Although, this demonstrate the differences in mesh requirements between the methodologies well.

The u-LAG model with a 10 µm element size, seen in Figure 7e, predicted the steady-state engagement thrust force and torque to within 3.5 % and 19 % error respectively. However, it should be noted that force evolution exhibits a very large amplitude of scatter about these mean values likely due to the mass scaling used which is required to reduce the computational cost. This model also did not consider any thermal effects due to the limitations discussed earlier making it not comparable with the other models, as well as not representing the physics of the process. Therefore, the updated Lagrangian with element deletion cannot be considered

appropriate for modelling the drilling process with large drill diameters. The apparent high accuracy of the u-LAG model at the studied set of cutting conditions is misleading and further investigation is required to determine the reason for this. This could possibly be due to the effect of modified stress triaxiality in the absence of the thermal effect on the damage initiation and evolution predictions.

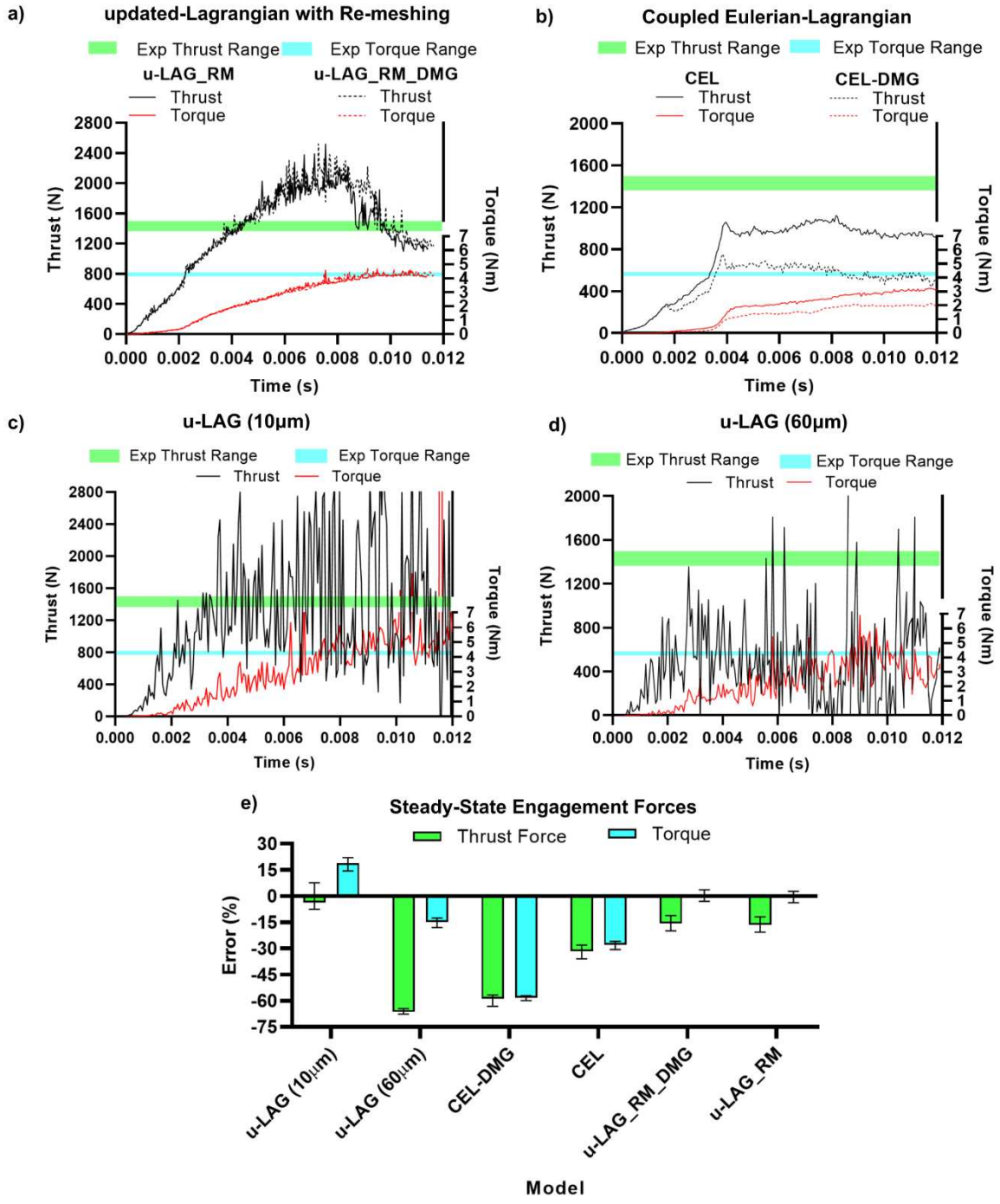

Figure 7: Evolution of the thrust force and torque predicted by the (a) updated-Lagrangian with re-meshing method, (b) coupled Eulerian-Lagrangian method, and the updated-Lagrangian with element deletion method with a (c) 10µm and (d) 60µm element sizes. The average steady-state thrust force and torque of the compared models are shown in (e).

4.2 Chip Morphology Analysis

Due to the complex chip geometry in drilling, it is difficult to precisely match the chip thickness measurement locations in the model to the experimental chips. However, the predicted chip thicknesses of each model were measured at a consistent time step during the steady-state tool engagement (after 0.01 s) at the top of the secondary shear zone and compared with the minimum and maximum experimental measurements (Figure 3), as shown in Figure 8. The u-LAG model with a 60 µm mesh did not produce a chip, as shown in Figure 9, so cannot be included in this comparison. The light grey band in Figure 8 represents the range of experimentally measured values, the light blue bar represents the u-LAG model with a 10 µm mesh, the green bars represent the CEL formulation models, and the red bars represent the updated-Lagrangian with dynamic re-meshing formulation models. The models without material damage implemented are indicated by a diagonal hatch pattern in the bars.

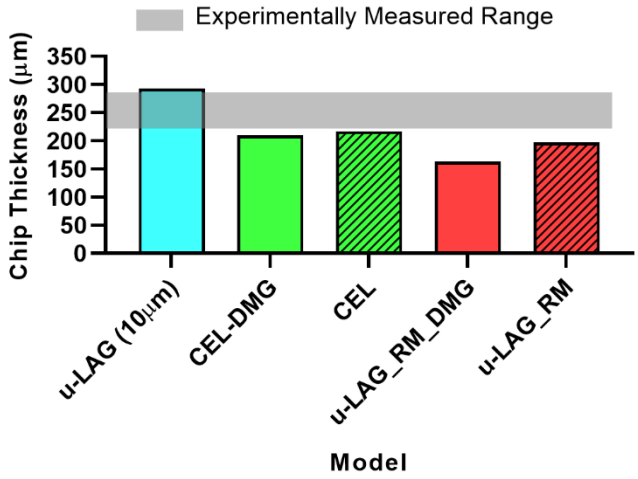

Figure 8: Predicted chip thicknesses compared with the experimentally measured range indicated by the grey band. A solid colour represents a model with damage implementation and the diagonal hatch pattern represents the models without.

The u-LAG_RM and CEL models both under predicted the chip thickness values with an error of approximately 15 % and 6.5 %, respectively, compared to the T_{min} value as shown in Figure 3c. Slightly thinner chips were predicted by the addition of material damage in both models increasing this error to about 30 % and 10 % for the u-LAG_RM_DMG and CEL-DMG models, respectively. The u-LAG model, however, predicted a larger chip thickness, exceeding the maximum experimentally measured value by 3.5 %. This is likely due to the lack of thermal softening effects.

The predicted chip morphology of the u-LAG models with a 10 µm and 60 µm element sizes is shown in Figure 9a and 9b, respectively. The model with 60 µm elements did not produce a chip due to the complete deletion of the large elements around the cutting edge as there was

not a sufficiently refined sacrificial layer of elements; indicating that this methodology requires a finer mesh than the other methodologies compared in this study to form a chip. Although the model with 10 µm elements did produce a chip, this had a significantly smaller radius of curvature compared with the other models and this was not observed in the experiment, Figure 3a.

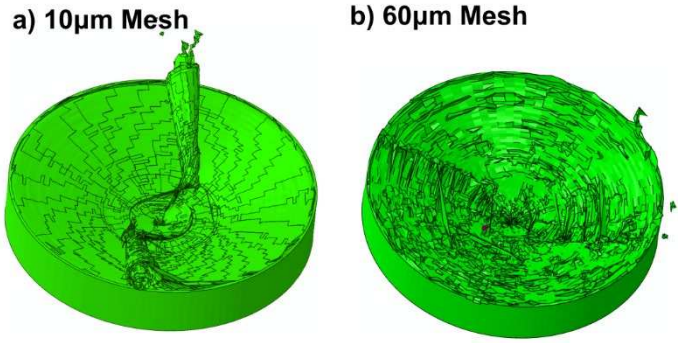

Figure 9: u-LAG model chip morphology with (a) 10µm and (b) 60µm element sizes.

Severe discontinuities were observed in the predicted chip geometry in the CEL and CEL-DMG models, shown in Figure 10a and 10c, at the initial stage of the chip formation as the tool enters the workpiece. This is because of the very small depth of cut as the tool first enters the workpiece coupled with a relativity coarse mesh in comparison. This prevents the initial flow of material around cutting edge from being simulated correctly due to the lack of required mesh resolution. As the depth of cut increases by further penetration of the drill into the workpiece, a complete continuous chip is formed. Additional simulations using the CEL model were carried out with an element size of 25 µm, although such a reduction in element size had minimal effect on the formation of these unrealistic features. Therefore, it is expected that a very fine mesh structure is required to prevent this phenomenon that will hinder the application of the CEL methodology in simulating large diameter hole drilling due to the associated computation cost.

4.3 Temperature Prediction

The implementation of material damage in CEL methodology caused a reduction in the predicted temperatures in the chip by approximately 200 °C in the CEL-DMG model compared to the CEL model in the primary shear zone, highlighted by the arrows in Figure 10c and 10a respectively. This is due the element softening of the damage model reducing the plastic work, and subsequently, reduced heat as a result of its conversion to the thermal energy. The predicted temperature distribution between the u-LAG_RM and u-LAG_RM_DMG models is very

similar, further demonstrating that the implementation of material damage in this methodology has a reduced impact compared to the impact on the CEL method.

The comparison of the CEL and u-LAG_RM models without material damage (Figure 10a and 10e) reveals that the CEL methodology predicts higher maximum temperatures, as indicated by the arrow in the Figure 10a. This higher temperature prediction would therefore cause an increase in the thermal softening effect and this potentially results in the reduction in the thrust force and torque seen in the CEL methodology compared with the updated-Lagrangian with dynamic re-meshing methodology. Similar observations on the higher temperature prediction by the CEL methodology compared with the updated-Lagrangian methodologies are also reported in [11], [20] for orthogonal cutting simulations. There are also significant differences in the predicted temperature distribution between the models, where the u-LAG_RM and u-LAG_RM_DMG models predict the higher temperature in the secondary shear zone, while in the CEL and CEL-DMG models this is observed in the primary deformation zone. The location of these maximum temperatures are indicated by arrows in the respective figures. This trend with respect to the location of the maximum temperatures is also observed in the cross-section of the chip. The difference in peak temperature site could be due to the smaller tool-chip contact area in the secondary shear zone of the CEL models, caused by a smaller predicted chip curvature radius that reduces the frictional work, and consequently, the temperature in the secondary shear zone.

The average temperatures in the cross section and on the surface of the chip outside of the primary and secondary shear zones in the chip are similar between the CEL and u-LAG_RM models, Figure 10a and 10e are indicative of this respectively. Although, the CEL model still predicts slightly higher temperatures following the same trends as the maximum temperatures.

On the other hand, the predicted temperatures on the cutting edge of the tool are approximately 300 °C higher in the updated-Lagrangian with dynamic re-meshing methodology (Figure 10f and 10h) compared to the CEL methodology (Figure 10b and 10d). This disparity could be linked to the control of the frictional heat partitioning between the tool and the workpiece available in the two methodologies, where more user control is granted in the latter in contrast to the former. Additionally, the maximum tool temperatures predicted in CEL and CEL-DMG models were at the outer edge of the tool, yet in the u-LAG_RM and u-LAG_RM_DMG models, these were in the centre of the cutting edge. This is reflected in the predicted chip

temperature distribution as these peak tool temperature locations correspond to the peak temperature locations on the chip.

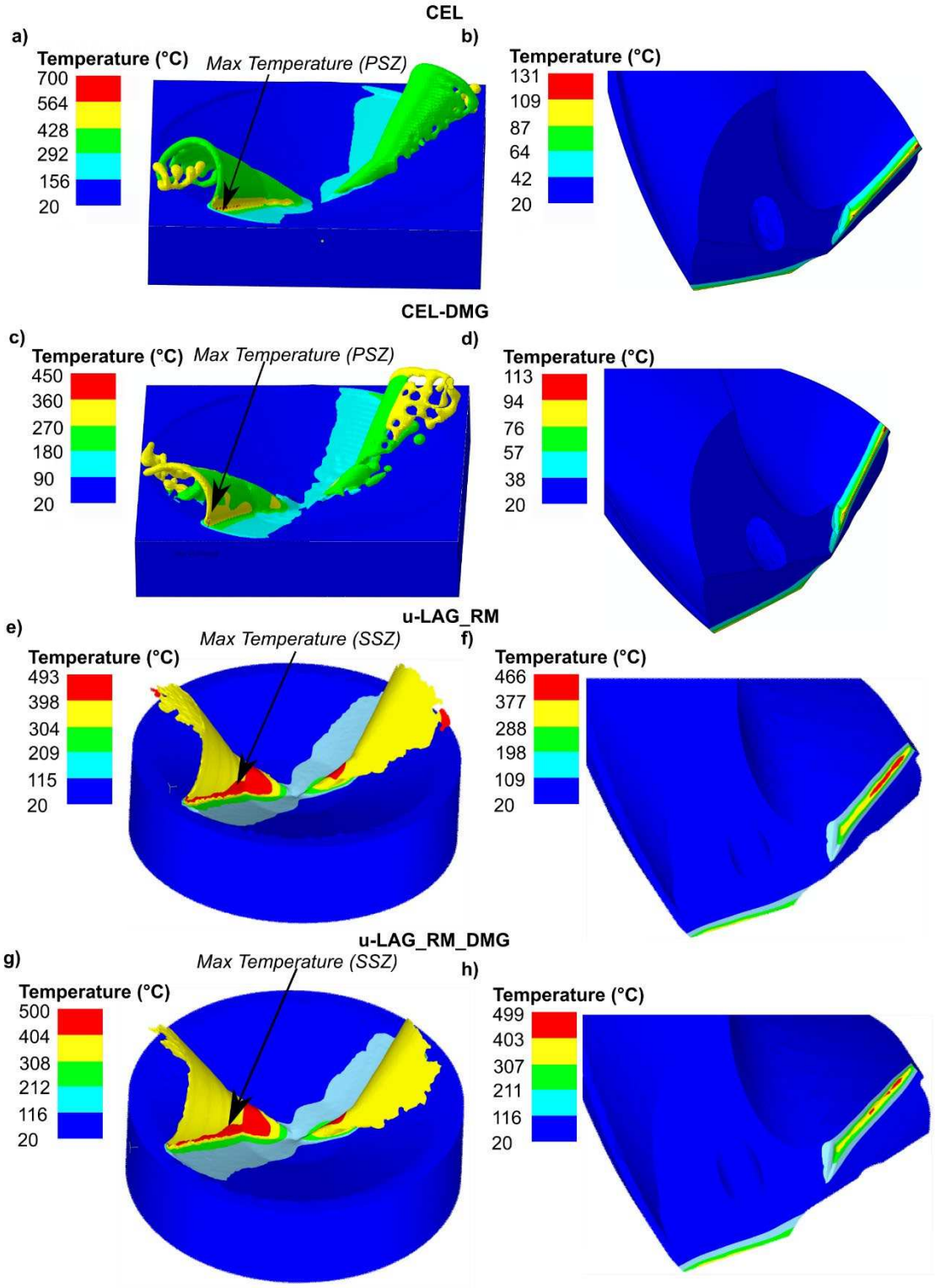

Figure 10: Predicted chip morphology and local temperature distribution of the (a-b) CEL, (c-d) CEL-DMG, (e-f) u-LAG_RM, and (g-h) u-LAG_RM_DMG models at the chip root and drill cutting edge. The arrows show the location of the maximum temperatures on the chip and whether it is in the PSZ or SSZ.

4.4 Computational Cost

The computational power available to each software package are reported in Table 5, unfortunately, there was a disparity between the available computational resources making it impossible directly compare the performance of the models. Nevertheless, the simulation times for each modelling methodology can be seen below in Table 6.

Table 5:
Computational Facilities

	ABAQUS/Explict Models	**DEFORM 3D Models**
CPU	Intel Xeon Gold 6138 (2.00GHz)	Intel Core i9-8950HK (2.9 GHz)
Number of Cores	20	6
RAM	64GB DDR4	16GB DDR4

Table 6:
Simulation Time Comparison

Model	**Simulation Total Step Time (s)**	**Simulation Run Time (hours)**	**Average Time Increment (s)**
u-LAG (10µm)	0.012	89.95	2.917×10^{-9}
u-LAG (60µm)	0.012	10.67	2.660×10^{-9}
CEL-DMG	0.012	86.00	3.120×10^{-9}
CEL	0.012	71.93	4.867×10^{-9}
u-LAG_RM_DMG	0.0118	39.48	2.000×10^{-6}
u-LAG_RM	0.0118	38.31	2.000×10^{-6}

The simulations times of the u-LAG_RM and u-LAG_RM_DMG models are considerably lower than those of the CEL and CEL-DMG models, even though much less computational power was used. This is likely due to the implicit numerical scheme used in DEFORM 3D which allowed stable time steps approximately 1000 times larger than that used in the explicit solver. Additionally, the use of adaptive re-meshing further reduced the number of total active as well as severely distorted elements in the model. The use of mass scaling to reduce simulation times is not possible in the CEL method as a Eulerian domain is used, this is a limitation of the ABAQUS software package [39].

The u-LAG model with a 60 µm element size results in a significantly reduced simulation time due to the 2000x mass-scaling used and that the solver is not thermally coupled, although as previously discussed this element size is too coarse for the methodology used. The u-LAG model with a refined 10µm element size, required to produce a chip, takes slightly longer than the CEL and CEL-DMG models, highlighting the impracticality of this methodology for 3D drilling further.

4.5 The Effect of Cutting Condition

The u-LAG_RM and CEL models were also compared at the higher cutting speed parameter set presented in Table 1, with the experimental thrust force and torque values. The force evolutions and the average steady-state force errors of each model are shown in Figure 11a and 11b respectively. The models with damage were not taken forward as this had a minimal impact on the updated-Lagrangian with dynamic re-meshing methodology and had a large negative impact on the accuracy of the thrust and torque prediction in the CEL methodology.

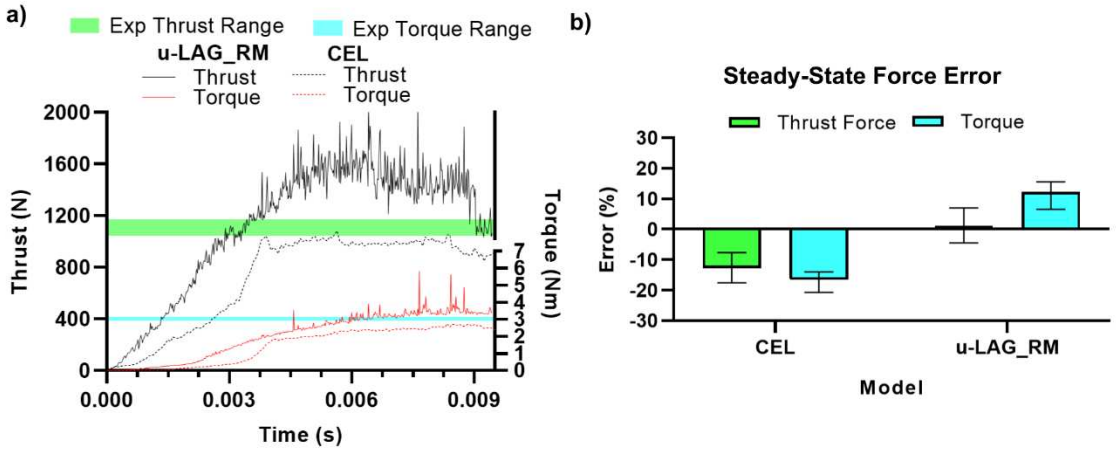

Figure 11: (a) Evolution of the thrust force and torque predicted by the updated-Lagrangian with re-meshing method and the coupled Eulerian-Lagrangian method. The solid lines represent the u-LAG_RM model and the dashed lines represent the CEL model, the thrust and thrust are represented by the red and black lines respectively. The average steady-state thrust force and torque of the compared models are shown in (b)

The CEL methodology under predicted the thrust force and torque at this cutting condition also, although the error is reduced by approximately 10 % compared to the previous parameter set, to within 20 % of both the experimental thrust and torque. The u-LAG_RM predicts higher steady-state torque and thrust forces than the CEL model, potentially due to predicting lower temperatures in the chip and workpiece which results in reduced thermal softening effects. The thrust force and torque values are both predicted to within 15 % of the experimentally measured values, as it did in the lower speed cutting condition with a better performance. The same trend in the thrust force evolution predicted by the u-LAG_RM model was also observed in this cutting condition, where the thrust force decreases when the torque reaches its maximum value, potentially linked to increased rate of thermal softening at maximum chip load as described previously.

Although the absolute values of error have reduced by approximately 10 % in the CEL model, the comparative trend with the DEFROM model is still representative, demonstrating that these

trends are potentially representative over a wide range of cutting conditions with varying cutting speeds and uncut chip thicknesses.

5 Conclusion

The results of the comparative study conducted to assess the performance of various modelling methodologies available to simulate the drilling process revealed that the updated-Lagrangian with element deletion methodology is not a computationally viable option for large diameter (>3 mm) drilling simulations. On the other hand, models not requiring element deletion for chip separation, including the updated-Lagrangian with dynamic re-meshing and the CEL methodologies, were able to fulfil the modelling with varied degree of accuracy. Therefore, although the u-LAG models have already been used and provide a reasonable accuracy with respect to the thrust force and torque prediction, care must be taken as the produced working models lack the fundamental physics of material deformation that results in unrealistic chip morphologies.

The updated-Lagrangian with dynamic re-meshing methodology is found to provide the most accurate predictions concerning the thrust force and torque, predicting these to within 15 %, at the lowest computational cost, while the CEL formulation was found to significantly under-predict these outputs and is considerably more computationally expensive to run. Therefore, the updated-Lagrangian with dynamic re-meshing methodology is the most suitable with regard to both accuracy and computational cost for simulating large diameter drilling.

The additional implementation of the Johnson-Cook damage model in the CEL formulation reduced the predicted thrust, torque, temperatures, and chip thickness. This considerably reduced the accuracy of the predicted thrust force and torque, indicating that care needs to be taken when tuning the displacement to failure value in the fracture model to the element size in this methodology. On the other hand, the implementation of the damage model was found to have no considerable effect on the predicted torque, thrust, and temperatures when using the updated-Lagrangian with dynamic re-meshing method. Although this did result in a thinner chip, following the same trend seen in the CEL methodology.

Acknowledgements

This research was funded by Sandvik Coromant and EPSRC (EP/L016257/1).

References

[1] R. Di Han and J. Wu, "Finite Element Simulation of Drilling Based on Third Wave Systems AdvantEdge," *Key Eng. Mater.*, vol. 431–432, pp. 229–232, 2010.

[2] Scientific Forming Technologies Cooperation, "DEFORM." 2020.

[3] Third Wave Systems, "Advantedge." 2020.

[4] Dassuault Systems, "Abaqus." 2020.

[5] M. Lotfi, S. Amini, and I. Y. Al-Awady, "3D numerical analysis of drilling process: heat, wear, and built-up edge," *Adv. Manuf.*, vol. 6, no. 2, pp. 204–214, 2018.

[6] F. Hu, L. Xie, J. Xiang, U. Umer, and X. Nan, "Finite element modelling study on small-hole peck drilling of SiCp / Al composites," *Int. J. Adv. Manuf. Technol.*, pp. 3719–3728, 2018.

[7] X. Nan, L. Xie, and W. Zhao, "On the application of 3D finite element modeling for small-diameter hole drilling of AISI 1045 steel," *Int. J. Adv. Manuf. Technol.*, vol. 84, no. 9–12, pp. 1927–1939, 2016.

[8] P. A. R. Rosa, P. A. F. Martins, and A. G. Atkins, "Revisiting the fundamentals of metal cutting by means of finite elements and ductile fracture mechanics," *Int. J. Mach. Tools Manuf.*, vol. 47, no. 3–4, pp. 607–617, 2007.

[9] M. R. Vaziri, M. Salimi, and M. Mashayekhi, "Evaluation of chip formation simulation models for material separation in the presence of damage models," *Simul. Model. Pract. Theory*, vol. 19, no. 2, pp. 718–733, 2011.

[10] M. Sadeghifar, R. Sedaghati, W. Jomaa, and V. Songmene, "A comprehensive review of finite element modeling of orthogonal machining process: chip formation and surface integrity predictions," *Int. J. Adv. Manuf. Technol.*, pp. 3747–3791, 2018.

[11] F. Ducobu, E. Rivière-Lorphèvre, and E. Filippi, "Application of the Coupled Eulerian-Lagrangian (CEL) method to the modeling of orthogonal cutting," *Eur. J. Mech. - A/Solids*, vol. 59, pp. 58–66, 2016.

[12] F. Ducobu and E. Filippi, "Finite element modelling of 3D orthogonal cutting experimental tests with the Coupled Eulerian-Lagrangian (CEL) formulation," *Finite Elem. Anal. Des.*, vol. 134, no. May, pp. 27–40, 2017.

[13] C. Zhang and H. Choi, "Study of segmented chip formation in cutting of high-strength lightweight alloys," *Int. J. Adv. Manuf. Technol.*, vol. 112, no. 9–10, pp. 2683–2703, 2021.

[14] F. Klocke, B. Döbbeler, B. Peng, and T. Lakner, "FE-simulation of the Cutting Process under Consideration of Cutting Fluid," *Procedia CIRP*, vol. 58, pp. 341–346, 2017.

[15] Y. Gao, J. H. Ko, and H. P. Lee, "3D coupled Eulerian-Lagrangian finite element analysis of end milling," *Int. J. Adv. Manuf. Technol.*, vol. 98, no. 1–4, pp. 849–857, 2018.

[16] A. Vovk, J. Sölter, and B. Karpuschewski, "Finite element simulations of the material loads and residual stresses in milling utilizing the CEL method," *Procedia CIRP*, vol. 87, pp. 539–544, 2020.

[17] A. M. Abdelhafeez, S. L. Soo, D. Aspinwall, A. Dowson, and D. Arnold, "A Coupled Eulerian Lagrangian Finite Element Model of Drilling Titanium and Aluminium

Alloys," *SAE Int. J. Aerosp.*, vol. 9, no. 1, pp. 2016-01–2126, 2016.

[18] P. J. Arrazola, T. Özel, D. Umbrello, M. Davies, and I. S. Jawahir, "Recent advances in modelling of metal machining processes," *CIRP Ann. - Manuf. Technol.*, vol. 62, no. 2, pp. 695–718, 2013.

[19] D. J. Benson and S. Okazawa, "Contact in a multi-material Eulerian finite element formulation," *Comput. Methods Appl. Mech. Eng.*, vol. 193, no. 39-41 SPEC. ISS., pp. 4277–4298, 2004.

[20] Y. Zhang, J. C. Outeiro, and T. Mabrouki, "On the selection of Johnson-Cook constitutive model parameters for Ti-6Al-4V using three types of numerical models of orthogonal cutting," *Procedia CIRP*, vol. 31, pp. 112–117, 2015.

[21] Simufact, "Material Data," 2020. [Online]. Available: https://www.simufact.com/material-data.html.

[22] G. Johnson and W. Cook, "A constitutive model and data for metals subjected to large strains, high strain rates and high temperatures," in *International Symposium on Ballistics ; 7*, 1983, pp. 541–547.

[23] S. A. Iqbal, P. T. Mativenga, and M. A. Sheikh, "Characterization of machining of AISI 1045 steel over a wide range of cutting speeds. Part 2: Evaluation of flow stress models and interface friction distribution schemes," *Proc. Inst. Mech. Eng. Part B J. Eng. Manuf.*, vol. 221, no. 5, pp. 917–926, 2007.

[24] G. Johnson and W. Cook, "Fracture Characteristics of Three Metals Subjected to Various Strains, Strain Rates, Temperatures and Pressures," *Eng. Fract. Mech.*, vol. 21, no. I, pp. 37–48, 1985.

[25] J. Ribeiro, A. Santiago, and C. Rigueiro, "Damage model calibration and application for S355 steel," *Procedia Struct. Integr.*, vol. 2, pp. 656–663, 2016.

[26] F. Ducobu, P. J. Arrazola, E. Rivière-Lorphèvre, G. O. De Zarate, A. Madariaga, and E. Filippi, "The CEL Method as an Alternative to the Current Modelling Approaches for Ti6Al4V Orthogonal Cutting Simulation," *Procedia CIRP*, vol. 58, pp. 245–250, 2017.

[27] S. P. F. C. Jaspers and J. H. Dautzenberg, "Material behaviour in conditions similar to metal cutting: Flow stress in the primary shear zone," *J. Mater. Process. Technol.*, vol. 122, no. 2–3, pp. 322–330, 2002.

[28] J. Borkovec, "Computer simulation of material separation process," Brno University of Technology, 2008.

[29] T. H. C. Childs, "Friction modelling in metal cutting," *Wear*, vol. 260, no. 3, pp. 310–318, 2006.

[30] S. Kato, K. Yamaguchi, and M. Yamada, "Stress Distribution at the Interface Between Tool and Chip in Machining," *J. Eng. Ind.*, vol. 94, no. 2, p. 683, 1972.

[31] W. Ben Salem, J. Rech, A. Dogui, H. Ben Abdelali, and P. Kapsa, "Numerical characterisation of the friction coefficient at the tool-chip-workpiece interface during friction tests of AISI 1045," *Int. J. Microstruct. Mater. Prop.*, vol. 9, no. 2, p. 147, 2014.

[32] K. Prakash Marimuthu, H. P. Thirtha Prasada, and C. S. Chethan Kumar, "Force, stress prediction in drilling of AISI 1045 steel using finite element modelling," *IOP Conf. Ser. Mater. Sci. Eng.*, vol. 225, 2017.

[33] K. Khalili and M. Safaei, “FEM analysis of edge preparation for chamfered tools,” *Int. J. Mater. Form.*, vol. 2, no. 4, pp. 217–224, 2009.

[34] Scientific Forming Technologies, *DEFORM User Manual v11.1*. .

[35] V. Norouzifard and M. Hamedi, “Experimental determination of the tool-chip thermal contact conductance in machining process,” *Int. J. Mach. Tools Manuf.*, vol. 84, pp. 45–57, 2014.

[36] F. Ducobu, E. Rivière-Lorphèvre, and E. Filippi, “On the introduction of adaptive mass scaling in a finite element model of Ti6Al4V orthogonal cutting,” *Simul. Model. Pract. Theory*, vol. 53, no. April, pp. 1–14, 2015.

[37] O. Isbilir and E. Ghassemieh, “Finite element analysis of drilling of titanium alloy,” *Procedia Eng.*, vol. 10, pp. 1877–1882, 2011.

[38] Y. Liu, M. Agmell, D. Xu, A. Ahadi, J. E. Stahl, and J. Zhou, “Numerical contribution to segmented chip effect on residual stress distribution in orthogonal cutting of Inconel718,” *Int. J. Adv. Manuf. Technol.*, vol. 109, no. 3–4, pp. 993–1005, 2020.

[39] Dassault Systèmes, “ABAQUS 6.14 User Manual.” 2021.